J Polym Environ (2012) 20:713–725
DOI 10.1007/s10924-012-0425-6

ORIGINAL PAPER

Effect of Silica Nanoparticles on the Mechanical Performances of Poly(Lactic Acid)

A. Dorigato · M. Sebastiani · A. Pegoretti · L. Fambri

Published online: 7 April 2012

Abstract Various kinds of fumed silica nanoparticles, different in terms of specific surface area and surface functionalization, were melt compounded with a poly(lactic acid) biodegradable matrix, with the aim to investigate the thermo-mechanical and optical properties of the resulting materials. Untreated nanoparticles at elevated surface area resulted to be effective in increasing elastic modulus, because of the extended filler–matrix interaction, while the finer dispersion of silica aggregates at the nanoscale obtained with surface treated nanoparticles led to noticeable improvements of the tensile properties at yield and at break, both under quasi-static and impact conditions. Also the fracture toughness and the creep stability were substantially enhanced by nanosilica addition, without impairing the original optical transparency of the matrix.

Keywords Poly(lactic acid) · Silica · Nanocomposites · Mechanical properties · Fracture · Creep

Introduction

In the last decades an increasing attention was devoted to the problem of waste disposal, especially for packaging materials. For this reason, extended efforts were made for the development of new materials, combining environmental sustainability and biodegradability or compostability [1–3]. Among various biodegradable polymers, aliphatic polyesters, such as poly(glycolic acid) (PGA), poly(lactic acid) (PLA), poly(ε-caprolactone) (PCL) and poly(3-hydroxybutyrate) (PHB), represent the most important family [4, 5]. In particular PLA, initially proposed by Kulkarni et al. [6] for surgical implants, has become the most promising polymer for various biomedical and industrial applications, due to the good balance of performances and degradation kinetics in dependence on the composition [7]. Moreover, poly(lactic acid) can be synthesized either from oil or from renewable resources [8], it is fully biocompatible and it possesses higher thermal, mechanical and optical properties with respect to other biodegradable polyesters [9]. From a chemical point of view, PLA is a homopolymer or a copolymer of L-lactic acid and/or D-lactic acid monomers. The final properties of PLA are related to the enantiomeric composition [9, 10]. Poly(L-lactic acid) (P-L-LA) and poly(D-lactic acid) (P-D-LA) are enantiomerically pure polymers, obtained from the polymerization of L-lactic acid and D-lactic acid, respectively. Because of their high stereoregularity, these are semicrystalline polymers with a melting temperature of about 180 °C [11]. On the other hand, poly(D,L-lactic acid) (P-D,L-LA), formally synthesized from equimolar mixture of L-lactic acid and D-lactic acid enantiomers, is a completely amorphous statistical copolymer with a glass transition temperature of about 50–60 °C [12]. Both melting temperature and crystalline content progressively decrease as the percentage of D lactic acid in copolymers increases, as shown in the case of poly-L,DL-lactide 70/30 [13].

From a mechanical point of view, PLA polymers behave as glassy and quite brittle materials, exhibiting a tensile modulus in the range 2–4 GPa and tensile strength of 30–50 MPa with deformation at break between 1 and 7 % in dependence on molecular weight, enantiomeric purity and crystallinity content [14–16].

A. Dorigato (✉) · M. Sebastiani · A. Pegoretti · L. Fambri
Department of Materials Engineering and Industrial Technologies and INSTM Research Unit, University of Trento, Via Mesiano 77, 38123 Trento, Italy
e-mail: andrea.dorigato@ing.unitn.it
URL: http://www.ing.unitn.it

The diffusion of PLA in the packaging industry was related to the development of low enantiomeric purity statistical copolymers, cheaper and suitable for traditional processes, such as extrusion and injection moulding [17]. These materials present good mechanical properties and excellent transparency, but they are relatively brittle and display low creep and thermal stabilities [7]. Polymer ductility and fracture toughness of PLA was improved by addition of synthetic plasticizers [18–20], such as various citrate esters [21], poly(ethylene glycol) [18], and poly(propylene glycol) [22]. On the other hand, plasticizers unavoidably play a detrimental role on material stiffness [20, 23]. Alternatively, PLA was blended with tough polymers, such as poly(ε-caprolactone) [24, 25], and other biodegradable polymers for biomedical applications [3–5, 14, 26], with a significant reduction of both the stress at yield and the dimensional stability at high temperatures. Moreover, the addition of significant amount of polyurethane elastomer [27, 28], or ethylene acrylate copolymer up to 20–30 wt% [29], was found to increase the toughness of the resulting blends.

The development of PLA filled with inorganic micro- and nanofillers represents another interesting possibility to increase both stiffness and thermal stability. In the first case, PLA composites were obtained by introduction of micrometric fillers, such as hydroxy apatite and calcium phosphate [30–35], calcium carbonate [36, 37], calcium sulfate [38–40] and talc [41] in between 5 and 25 wt%. On the other hand, it is widely proven that the introduction of small amounts of nanostructured materials may represent an effective way to enhance the mechanical performances of thermoplastics. Inorganic nanoparticles have been often added to polymeric matrices to improve their toughness and strength, to increase their thermal stability and to enhance the barrier properties of the pristine polymer. For as concern poly(lactic acid) based nanocomposites, layered silicates (nanoclays) were the most frequently utilized [42–49], but also inorganic nanoparticles were considered. In fact, Luo et al. [50] added grafted titania (g-TiO_2) nanoparticles to a poly(lactic acid) matrix to prepare PLA/TiO_2 nanocomposites via melt processing, finding that both matrix crystallinity and mechanical properties were improved. Jang et al. [51] prepared melt extruded PLA nanocomposites containing nano-sized precipitated calcium carbonate and organically modified montmorillonite, showing significantly different effects on the strength, modulus and elongation at break depending on the filler type. Cao et al. [52] investigated the crystallization of a poly(L-lactic acid)/silica nanocomposite prepared through in situ melt polymerization of L-lactic acid in the presence of acidic silica sol, finding that silica nanoparticles acted as nucleation agents in the PLLA matrix and enhanced its nucleation and overall crystallization rates, especially at high crystallization temperatures. Zhang et al. [53] synthesized poly(lactic acid)/fumed silica nanocomposites by melt compounding in a twin-screw extruder, and studied their thermal properties through experiments and molecular dynamics simulations. From a general point of view, the direct mixing of silica nanoparticles with PLA resulted in their aggregation, with the consequent deterioration of the mechanical properties. In order to overcome this problem, they propose to modify the silica particles with a surfactant or with silane-coupling agents. Yan et al. [54] reported on the surface modification of silica nanoparticles with a L-lactic acid oligomer by direct grafting onto the surface silanol groups of the silica nanoparticles, showing that the toughness and the tensile strength of the poly(L-lactic acid) matrix was greatly improved, because of the good dispersion of silica nanofiller. Zhu et al. [55] prepared melt mixed poly(lactic acid) based nanocomposites adding oleic acid treated fumed silica nanoparticles. It was found that even a low concentration of organomodified nanoparticles (i.e. less than 1 wt%) produced an evident plasticizing effect, thus improving the flexibility of the PLA matrix. More recently, the biodegradation of PLA- fumed silica nanocomposites has been investigated [56]. PLA and its nanocomposites were degraded in compost at 58 °C; at this temperature all samples presented a significant level of polymer degradation, but a certain protection action of silica towards PLA degradation was observed. Mass loss induction time for PLA (20 days) was considerably shorter than that of 5 wt% nanosilica filled samples (30–35 days).

A systematic investigation on the effect of silica nanoparticles, of various surface area, surface treatment and content, on the mechanical performances of poly(lactic acid) is not available in the open literature. Therefore, in this work various amounts of fumed silica nanoparticles, having different surface properties, were melt compounded to a PLA matrix utilized in the packaging industry. Particular attention was devoted to the tensile and fracture behaviour of the composites, both under quasi-static and impact conditions. The optical behaviour of the resulting composites was also investigated.

Experimental Section

Materials and Sample Preparation

Poly(lactic acid) granules supplied by NaturePlast (Caen, France) and commercialized under the trade name of PLE 005 (MFI at 190 °C and 2.16 kg = 16 g (10 min)$^{-1}$, density = 1.25 g cm^{-3}), were utilized as matrix. PLE 005 exhibited an intrinsic viscosity of 1.35 g dl^{-1} (Ubbelhode viscosimeter in chloroform at 25 °C) and an enantiomeric content of L-lactic acid of about 94 wt% and D-lactic acid

of about 6 wt% as determined through an Opthec PL1 polarimeter. Various kinds of fumed silica nanoparticles, supplied by Evonik (Hanau, Germany), were utilized as nanofillers. In particular, Aerosil® 90, Aerosil® 200 and Aerosil® 380 are hydrophilic fumed silica nanoparticles, having respectively a nominal specific surface area of 90, 200 and 380 $m^2\ g^{-1}$. Aerosil® r805 is a hydrophobic fumed silica, obtained by treating Aerosil® 200 with octylsilane ($-C_8H_{17}$), while Aerosil® r816 is obtained from Aerosil® 200 after a surface modification with hexadecylsilane ($-C_{16}H_{33}$). Density of the nanosilicas was measured through a Micrometrics Accupyc® 1330 helium pycnometer, while their specific surface area (SSA) values were determined by an ASAP® 2010 (Accelerated Surface Area and Porosimetry) machine, according to the Brunauer–Elmett–Teller (BET) procedure. Table 1 summarizes experimental density and SSA values of the fumed silica nanoparticles utilized in this work. Both polymeric granules and nanofillers were utilized as received.

The nanofillers and the matrix were melt compounded in PolyLab Rheomix R600 internal mixer (Thermo Haake GmbH, Germany) at 160 °C for 10 min and 90 rpm. The resulting materials were then pressed through a Carver® laboratory press at 160 °C for 5 min at low pressure (0.9 MPa). In this way square sheets with a side of 200 mm and a thickness of 0.8 mm were produced. Some thicker (4 mm) samples were also obtained for fracture mechanics analysis. First of all, nanocomposite filled with the various typologies of fumed silica nanoparticles at a constant filler loading of 2 vol% were prepared. Considering that Aerosil® 380 and Aerosil® r805 filled nanocomposite displayed the most interesting properties under ramp quasi-static tensile tests, these nanofillers were chosen for the preparation of samples at different silica contents, ranging from 1 to 24 vol%. The unfilled matrix was denoted as PLA, while nanocomposites were designated indicating the matrix, the kind of filler and its amount. For instance, a sample filled with 2 vol% of Aerosil® 200 is indicated as PLA-A200-2.

Experimental Techniques

Differential scanning calorimetry (DSC) tests were performed by using a Mettler® DSC30 calorimeter by using a cycle of heating–cooling–heating in the range 0–200 °C at ± 10 °C min^{-1} under a nitrogen flow of 100 mL min^{-1}. The crystallinity content (C) was computed from the melting enthalpy (ΔH_m) and normalized by the standard enthalpy of the fully crystalline PLLA (ΔH_0), taken as 93.6 J g^{-1} [57], according to the following Equation:

$$C = (100 - f) \cdot \frac{\Delta H_m}{\Delta H_0} \quad (1)$$

where f is the weight percentage of the filler.

Quasi-static tensile tests under ramp loading (constant strain rate) were performed at 25 °C by using an Instron® 4502 tensile testing machine on ISO 527 1BA dogbone samples, 5 mm wide and 0.8 mm thick. Elastic modulus was evaluated at a crosshead speed of 0.25 mm min^{-1}, and the strain was recorded through an Instron 2620-601 extensometer, having a gage length of 12.5 mm. According to ISO 527 standard, the elastic modulus was determined as a secant value between deformation levels of 0.05 and 0.25 %. Quasi-static tensile tests at break were conducted at a crosshead speed of 1 mm min^{-1} without extensometer, and the deformation was monitored normalizing the crosshead displacement for the gage length of the samples (30 mm). In this way the quasi-static tensile properties at yield (σ_y) and at break (σ_b, ε_b) were determined. Specific tensile energy to break (TEB) under quasi-static conditions was computed integrating the stress–strain curves. At least five specimens were tested for each sample.

The maximum tensile stress (σ_{max}), the strain at break (ε_b) and the specific tensile energy to break (TEB) were also determined under impact conditions. Tensile impact tests were conducted on ISO 527-1BA specimens with a CEAST instrumented impact pendulum at a speed of 1.0 m s^{-1}, at an impact energy of 1.83 J. Five specimens were tested for each sample.

Table 1 Density, specific surface area (SSA), and estimated mean diameters of fumed silica nanoparticles utilized in this study

Nanofiller type	Density[a] (g cm^{-3})	BET surface area[b] ($m^2\ g^{-1}$)	Estimated mean particles diameter (nm)
A90	2.50 ± 0.01	99.5 ± 0.7	20
A200	2.27 ± 0.02	196 ± 1.7	12
A380	2.41 ± 0.02	320.8 ± 3.4	7
Ar805	1.84 ± 0.01	151.7 ± 0.8	12
Ar816	2.04 ± 0.01	159.2 ± 1.3	12

[a] Measured through a Micrometrics Accupyc® 1330 helium pycnometer

[b] Measured through ASAP® 2010 Accelerated Surface Area and Porosimetry machine

In order to gain more detailed information on the fracture behaviour of the investigated materials, a fracture mechanics approach based on the J-integral [58] was adopted. According to ASTM D6068 standard [59], single edge notched bending (SENB) samples (4 mm thick, 10 mm wide and 60 mm long) were tested at a crosshead speed of 1 mm min^{-1}. The distance between the grips was 52 mm, while a sharp notch 5 mm deep was produced in the middle section of the samples. Following the multi-specimen method, specimens were loaded to various displacement levels and then cryofractured in liquid nitrogen, in order to evaluate the resulting crack propagation length (Δa) through optical microscope photographs. The energy (U) required to produce a certain crack propagation (Δa) was evaluated from the integration of force–displacement curves (U_t), subtracting the indentation energy (U_{ind}), measured on un-notched specimens. The J integral was then computed as follows [59]:

$$J = \frac{\eta U}{B(W - a_0)} \tag{2}$$

where η is a parameter depending on the testing configuration (2 for SENB specimens), B and W are respectively the thickness and the width of the samples, a_0 is the initial notch length. The J–R curves were therefore constructed considering J values at various crack propagation lengths, and the data fitted according to the following equation [59]:

$$J = C_1 \cdot (\Delta a)^{C_2} \tag{3}$$

where C_1 and C_2 are constants determined a posteriori from the fitting of J–R curves. Therefore, according to the ESIS protocol [60] a fracture initiation J_C parameter was computed as the J value corresponding to a crack propagation of 0.2 mm.

Short term (3,600 s) creep tests were performed at 30 °C by using an Instron® 4502 testing machine. Rectangular specimens 100 mm long, 5 mm wide and 0.8 mm thick were utilized, setting a gage length of 60 mm. A tensile creep compliance $D(t)$ was computed by dividing the time dependent strain $\varepsilon(t)$ by the constant applied stress σ_0. Samples were tested at various stress levels, from 5.1 to 25.7 MPa, i.e. in a range between 10 % and the 50 % of the stress at yield of neat PLA. Isochronous curves at different times (600, 1,800 and 3,600 s) were then constructed. The Burgers model was utilized to analyze the creep data. This mechanical model, depicted in Fig. 1, consists of a series combination of a Maxwell and a Kelvin element, and its constitutive equation reads:

$$D(t) = \frac{1}{E_M} + \frac{1}{E_K}\left[1 - \exp\left(-\frac{E_K}{\eta_K}t\right)\right] + \frac{t}{\eta_M} \tag{4}$$

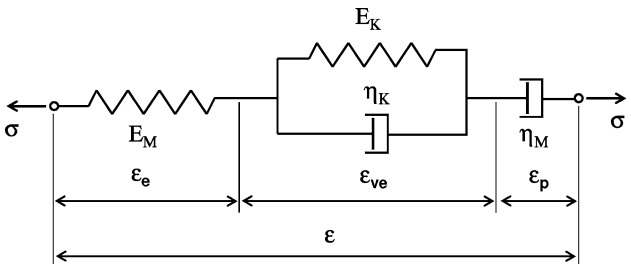

Fig. 1 Schematic representation of the Burgers model

where E_K and η_K represent the elastic and the viscous components in the Kelvin model, while E_M and η_M represent analogous parameters for the Maxwell model, respectively. The first term of Eq. (4) describes the instantaneous elastic compliance related to the Maxwell model, while the second term represents the delayed viscoelasticity of the Kelvin component. The third term describes the irreversible viscous flow in the course of creep, if any.

Field emission scanning electron microscopy (FESEM) observation were performed through a Zeiss Supra 40 microscope, operating at an acceleration voltage of 10 kV on cryofractured specimens. The transparency of the samples was qualitatively evaluated on 0.8 mm thick specimens by digital pictures taken by a Nikon Coolpix® 4500 photocamera. In addition, UV spectroscopy measurements were performed on 0.5 mm thick specimens by a Jasco® V570 spectrophotometer, in a wavelength interval between 200 and 800 nm and a scan speed of 200 nm min^{-1}. The transmittance (T) as a function of the wavelength (λ) was determined.

Results and Discussion

DSC Analysis

Figure 2 reports DSC thermograms collected during the first heating stage of pure PLA and of nanocomposites with a constant filler content of 2 vol%, while the most important thermal parameters (such as glass transition, melting temperatures and percentage of crystallinity) are summarized in Table 2. Pure PLA sample shows a glass transition temperature at about 60 °C, while the melting peak is located at about 140 °C. Considering that the intensity of the melting peak is practically negligible (crystallinity of about 0.5 %), this materials can be considered amorphous. From Fig. 2 it can be observed that the addition of 2 vol% of fumed silica nanoparticles does not significantly affect the glass transition temperature of the material, which results to be about 60 °C in the first and about 59 °C in the second heating scan. Furthermore, these types of

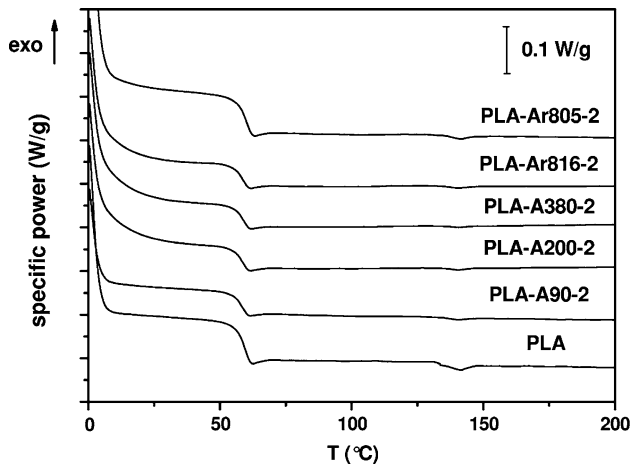

Fig. 2 DSC thermograms (first heating) of neat PLA and 2 vol% filled PLA nanocomposites

nanofillers do not show any appreciable nucleating effect on the polymeric matrix, being the crystalline amount of the nanofilled samples practically equal to that of the unfilled matrix. Moreover, DSC data obtained during the second heating cycle (Table 2) show how the thermal properties of the investigated samples are not substantially affected by their thermal history. Our observations are in rather good agreement with the study of Zhang et al. [53] on the thermal properties of poly(lactic acid)/fumed silica nanocomposites in which a very little increase in T_g (1.3 °C) has been reported. In a recent study, Fukushima et al. [56] observed that dispersed fumed silica nanoparticles dispersed in a PLA matrix can decrease the extent and kinetic of crystallization of PLA upon heating.

Tensile Behavior Under Ramp Loading

Representative stress–strain curves of quasi-static tensile tests under ramp loading (constant strain rate) of pure PLA and relative nanocomposites at a filler loading of 2 vol% are compared in Fig. 3a, while the most important mechanical parameters obtained from these tests are collected in Table 3. According to our previous experience, fumed silica nanoparticles resulted to be very effective in enhancing the elastic modulus of polymer matrices, such as low density polyethylene [61], poly(methyl pentene) [62] or cycloolefin copolymers [63]. Nevertheless, is evident that the introduction of fumed silica nanoparticles in the PLA matrix under investigation produces only a slight increase of the elastic modulus. When untreated fumed silica nanoparticles are added, the stiffening effect is proportional to the nanofiller surface area, while the surface functionalization of silica nanoparticles does not play a role on the elastic properties of the resulting materials. In fact, if standard deviation values are taken into account, elastic moduli of PLA-Ar805-2 and PLA-Ar816-2 nanocomposites are virtually the same of PLA-A200-2. The stress at yield (σ_y) slightly increases with the nanosilica introduction, especially when organo-modified silicas are utilized. It is worthwhile to note that an enhancement of σ_y is generally interpreted as an indication of good filler -matrix interaction [64–66]. Even the stress at break (σ_b) is slightly improved by nanoparticles addition, but with a less clear dependency from nanofiller surface properties. More interestingly, the introduction of hydrophilic (untreated) fumed silica nanoparticles produces a slight decrease of the strain at break, while surface treated nanoparticles are able to remarkably increase the elongation at break (ε_b). For instance, ultimate elongation of PLA-Ar805-2 nanocomposite is about 50 % higher than that of pure PLA. As suggested by Zhang et al. [67], we could hypothesize that the presence of a surface treatment decreases the surface energy of the nanoparticles, resulting in a decreasing interaction with the polymer matrix and a possible lubricating effect on it. The enhancement of the strain at break detected for surface treated silica filled nanocomposites is responsible of a noticeable improvement of the specific tensile energy at break (TEB) adsorbed under quasi-static conditions. In fact, TEB value of PLA-Ar805-2 nanocomposite is 77 % higher than that displayed by pure PLA. From these preliminary investigation, it emerges that Aerosil ® 380 produces the highest increase in tensile

Table 2 Results from DSC tests on neat PLA and 2 vol% filled nanocomposites

Sample	First heating			Cooling	Second heating		
	T_g (°C)	T_m (°C)	C (%)	T_g (°C)	T_g (°C)	T_m (°C)	C (%)
PLA	59.6	141.2	0.6	54.0	59.4	141.8	0.4
PLA-A90-2	60.5	141.1	1.2	54.3	57.7	140.2	0.2
PLA-A200-2	61.7	140.4	0.6	51.6	58.2	140.5	0.2
PLA-A380-2	62.0	140.0	0.6	53.6	58.5	140.5	0.1
PLA-Ar805-2	60.4	141.2	1.0	53.8	59.9	141.6	0.4
PLA-Ar816-2	61.9	141.3	0.5	53.6	58.2	140.7	0.2

T_g glass transition temperature, T_m melting temperature, C crystalline content

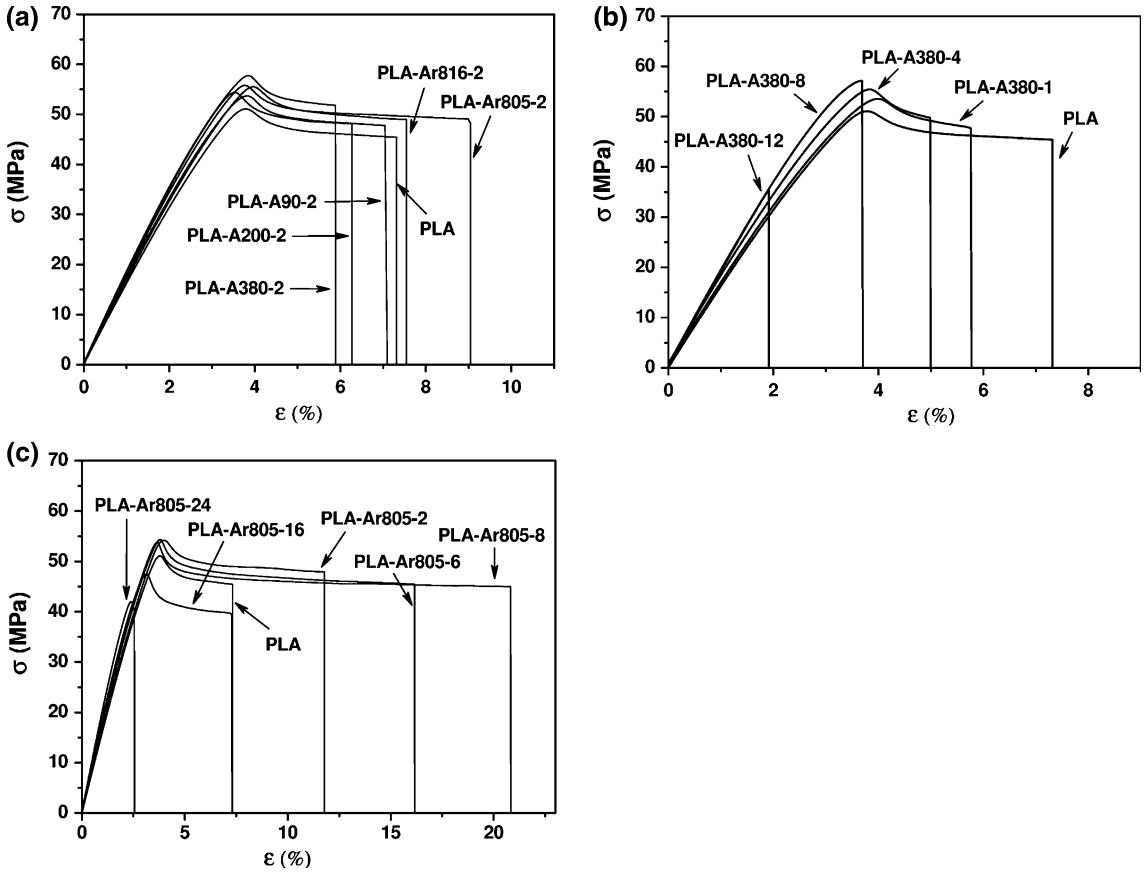

Fig. 3 Representative stress–strain curves of quasi-static tensile tests of neat PLA and relative nanocomposites. **a** 2 vol% filled samples, **b** PLA-A380-x ($x = 1 - 12$ vol%) and **c** PLA-Ar805-x nanocomposites ($x = 1 - 24$ vol%)

Table 3 Quasi-static tensile properties of PLA and 2 vol% filled nanocomposites

Sample	E (GPa)	σ_y (MPa)	σ_b (MPa)	ε_b (%)	TEB (MJ m^{-3})
PLA	3.31 ± 0.22	51.3 ± 1.0	45.5 ± 0.7	7.79 ± 0.58	2.99 ± 0.31
PLA-A90-2	3.49 ± 0.10	53.7 ± 1.6	48.0 ± 0.7	6.87 ± 1.65	2.66 ± 0.72
PLA-A200-2	3.52 ± 0.15	52.1 ± 1.6	47.2 ± 0.9	5.85 ± 0.32	2.17 ± 0.16
PLA-A380-2	3.62 ± 0.09	55.1 ± 0.7	49.1 ± 1.4	5.56 ± 0.84	2.10 ± 0.44
PLA-Ar805-2	3.58 ± 0.13	55.2 ± 1.9	48.0 ± 1.8	11.91 ± 0.37	5.30 ± 0.31
PLA-Ar816-2	3.37 ± 0.14	57.0 ± 1.5	50.0 ± 1.3	8.51 ± 0.99	3.46 ± 0.38

modulus, whereas Aerosil® r805 is responsible of the largest increment in elongation and tensile energy at break. Therefore, these nanofillers are selected for a deeper investigation involving the preparation of nanocomposites with various filler amounts from 2 to 24 vol%. Representative stress–strain curves of PLA nanocomposites filled with various amounts of Aerosil® 380 and Aerosil® r805 nanoparticles are respectively reported in Fig. 3b, c, while their quasi-static tensile properties are summarized in Fig. 4. Elastic modulus increases with the volume fraction of both fillers (Fig. 4a), but the stiffening effect is more pronounced when untreated nanoparticles are added. In the case of Aerosil® 380 the maximum volume fraction is limited to 12 % because at higher content the material becomes too brittle. The lower stiffening effect provided by Aerosil® r805 nanoparticles can be attributed both to their lower surface area and to the presence of a soft organic surface layer whose stiffness is probably lower than that of bulk PLA matrix. As documented in Fig. 4b, stress at yield presents a maximum at low filler content ($\Phi = 2$ vol% for Aerosil® 380 and $\Phi = 1$ vol% for Aerosil® r805) and then it decreases, probably due to nanofiller aggregation. In fact, ultimate properties strongly depend on microstructure (i.e. filler aggregation) and interaction. Samples filled with

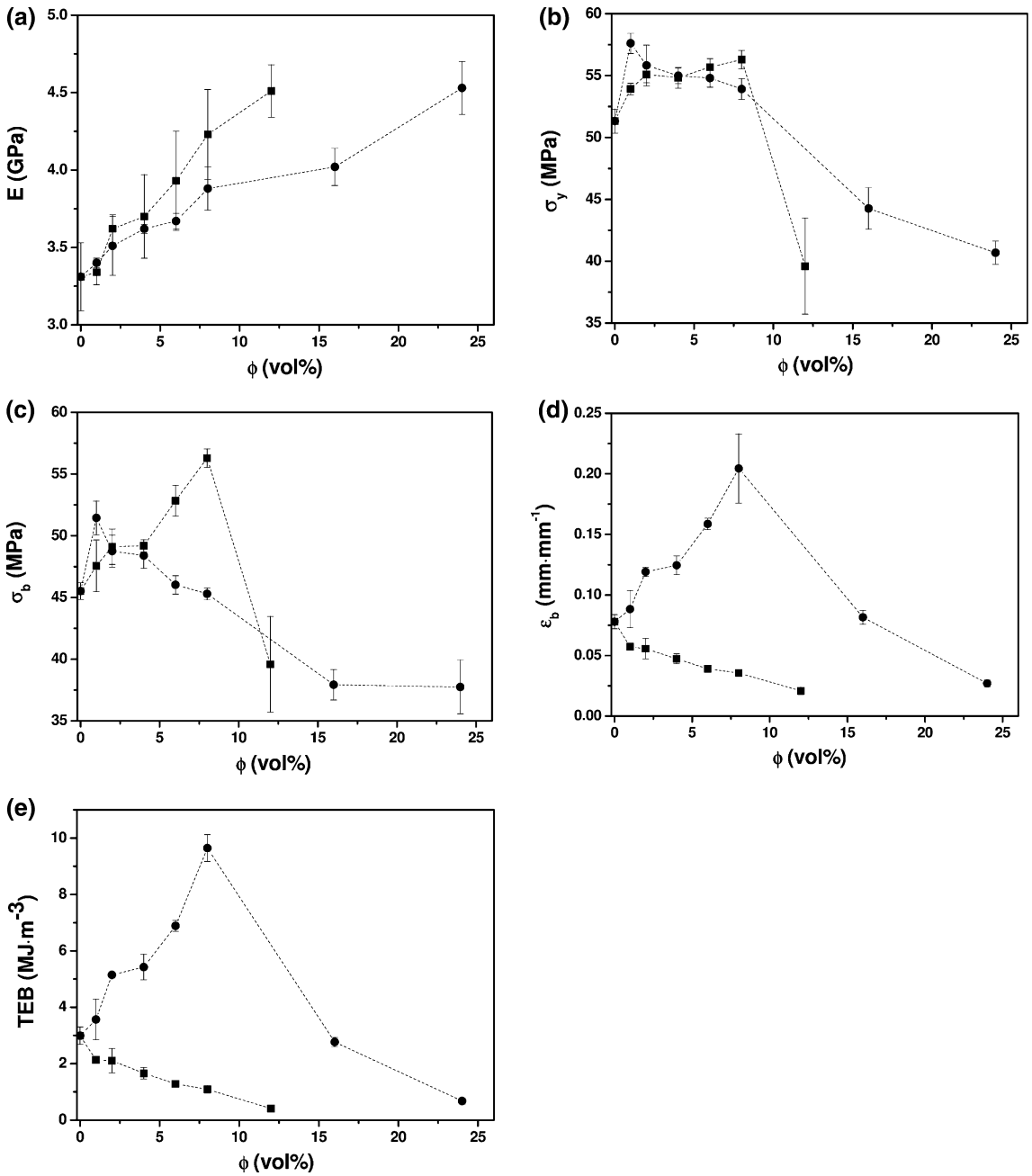

Fig. 4 Quasi-static tensile properties of (*filled square*) PLA-A380-x ($x = 1 - 12$ vol%) and (*filled circle*) PLA-Ar805-x ($x = 1 - 24$ vol%) nanocomposites. **a** Elastic modulus E, **b** stress at yield σ_y, **c** stress at break σ_b, **d** strain at break ε_b, **e** specific tensile energy to break TEB

untreated nanoparticles show a very steep σ_y drop for silica content higher than 8 vol%, while Aerosil® r805 filled nanocomposites are characterized by a more gradual σ_y decrease at elevated filler amounts. This difference can be probably ascribed to the different aggregation state of silica nanoparticles within the matrix due to surface organomodification. Similar considerations can be extended to stress at break data (Fig. 4c). The effect of the nanoparticles type on the tensile properties of the prepared composites is particularly evident when strain at break (Fig. 4d) and specific tensile energy to break (Fig. 4e) values are considered. While Aerosil® 380 provokes a progressive embrittlement of the PLA matrix, Aerosil® r805 induces a remarkable increase of strain at break values up to a filler content of 8 vol%, after which a sudden embrittlement is observed. It is worthwhile to note that in the work of Zhu et al. [55] the strong enhancement of the PLA strain at break due to the presence of the oleic acid functionalization on the surface of fumed silica nanoparticles was counterbalanced by an heavy reduction of the tensile strength even

at high filler contents. In our case the remarkable enhancement of the ultimate strain is accompanied by a slight increase of the stress at break.

Evaluation of Filler–matrix Interaction

The effect of the polymer-filler interaction and of nanofiller aggregation can be quantitatively described with the help of a model developed by Pukanszky and co-workers [68, 69] for particulate filled composites. In particular, the dependency of the tensile yield stress on the filler volume fraction Φ can be expressed as:

$$\sigma_y = \sigma_{y0}\frac{1-\Phi}{1+2.5\Phi}\exp(B\Phi) \quad (5)$$

where σ_y and σ_{y0} are the yield stress of the composite and the matrix, respectively, while B is a term related to the load carrying capability of the filler and it depends on filler–matrix interaction. The term $(1-\Phi)/(1+2.5\ \Phi)$ expresses the effective load-bearing cross-section of the matrix. At zero interaction ($B = 0$), the entire load is carried by the polymer and the load-bearing cross-section decreases with increasing filler content. As mentioned before, B is influenced by all factors affecting the load-bearing capacity of the filler, i.e. on the strength of interaction (which in turn depends on the surface energy/chemistry of the constituents) and on the size of the contact surface. Therefore, B can be expressed as follows:

$$B = (1 + A_f\rho_f l)\ln\left(\frac{\sigma_{yi}}{\sigma_{y0}}\right) \quad (6)$$

where A_f is the specific surface area of the filler (contact surface), ρ_f is its density, while l and σ_{yi} are the thickness and the yield stress of the interphase, respectively. It is obvious that the latter two parameters strongly depend on the strength of matrix-filler interaction. Therefore, a linear relationship exists between the natural logarithm of reduced yield stress σ_{yred} (defined as follows) and the filler content:

$$\ln\sigma_{yred} = \ln\sigma_y\frac{1-\Phi}{1+2.5\Phi} = \ln\sigma_{y0} + B\Phi \quad (7)$$

Reduced yield stress values for nanocomposites filled with Aerosil® 380 and Aerosil® r805 fumed silica are plotted as a function of the filler concentration in Fig. 5, while the parameters resulting from the fitting with Eq. (7) are collected in Table 4. It is evident that Pukanszky model adequately fits our experimental data up to a silica content of 8 vol%. For higher silica amounts, samples filled with Aerosil® 380 break before yielding, probably because of the filler aggregation and the stronger interaction compared to composites prepared with functionalized nanoparticles. Nanocomposites filled with Aerosil® r805 show matrix yielding even at elevated filler contents. However, a strong

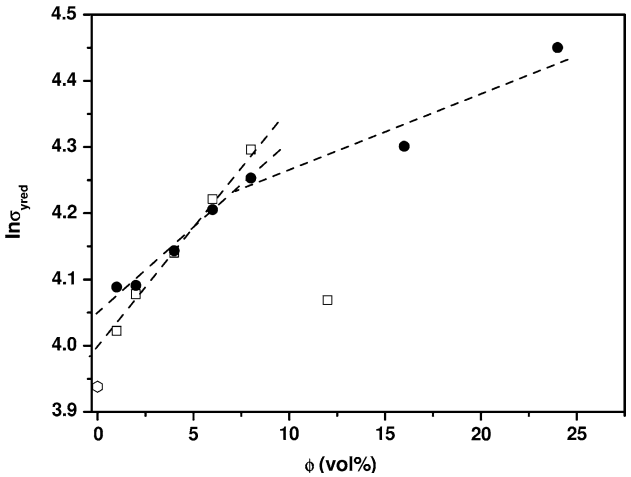

Fig. 5 Reduced stress at yield data of (*square*) PLA-A380-x ($x = 1 - 12$ vol%) and of (*filled circle*) PLA-Ar805-x ($x = 1 - 24$ vol%) nanocomposites, with the fitting lines according to Pukanszky model [(Eq. 7)]. *Circle* Reduced stress at yield of the neat PLA

Table 4 Fitting parameters of stress at yield data of PLA-A380-x and PLA-Ar805-x nanocomposites according to the Pukanszky model [Eq. (7)]

Sample	ln σ_{y0}*	σ_{y0} (MPa)*	B*	R^2
PLA	3.94	51.3	–	–
PLA-A380-x	3.99	54.1	3.8	0.997
PLA-Ar805-x	4.05	57.4	2.5	0.984

* Data were fitted up to a filler loading of 8 vol%

deviation from the initial linear trend can be detected for filler fractions higher than 8 vol%, probably as a consequence of filler aggregation. In fact, the reduction of the filler–matrix interfacial area due to silica agglomeration at elevated filler amounts could be responsible of a noticeable decrease of the filler–matrix interaction. In these conditions, the reinforcing capability of the silica nanoparticles at elevated nanofiller amounts is reduced.

The different slope of fitting lines, expressed by B values reported in Table 4, accounts for a difference in polymer-filler interaction. For composites prepared by using untreated nanoparticles a B value of 3.8 is determined, while σ_{yred} data of Aerosil® r805 filled samples are fitted by using a lower B value (2.5). The B values found for the materials under investigations lie within the range typically reported in the scientific literature for particulate composites, i.e. between 1.7 and 13.0 [68]. The obtained B values confirm our hypothesis of lower filler–matrix interaction for surface treated nanoparticles with respect to untreated ones. The value of the intercept of reduced stress for $\Phi = 0$ (σ_{y0}) also slightly changes upon silica addition, especially when functionalized nanoparticles are utilized.

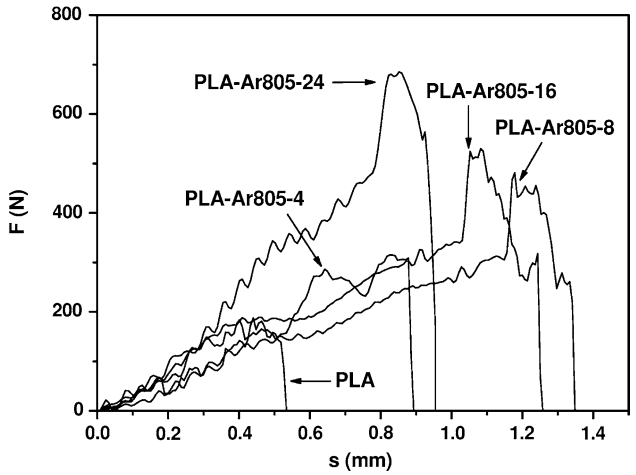

Fig. 6 Representative force–displacement curves of PLA-Ar805-x nanocomposites under tensile impact conditions ($x = 1 - 24$ vol%)

The change of the matrix properties due to nanofiller addition is well known in literature, and it is often attributed to a change in glass transition temperature or in the crystallinity type and/or amount [68, 70]. In the present case, no differences in the T_g or in the crystalline fraction are detected from DSC analysis.

Impact and Fracture Mechanics Response

Due to the interesting toughening effects observed when Aerosil® r805 nanoparticles are added to the PLA matrix a more detailed investigation of the fracture behaviour has been performed. Representative force–displacement curves under tensile impact conditions on Aerosil® r805 filled nanocomposites are reported in Fig. 6, while in Table 5 the most relevant results are summarized. Maximum tensile stress (σ_{max}) markedly increases up to a filler concentration of 16 % and then decreases. Strain at break and specific tensile energy to break values present a maximum for a silica loading of 6 and 8 vol%, respectively. It is worthwhile to observe that TEB value for PLA-Ar805-8 nanocomposite is 6 times higher than that of neat PLA matrix. Considering that PLA-Ar805-8 nanocomposite shows the highest TEB value both under quasi-static and impact conditions, the fracture behaviour of this material and neat PLA are investigated through an elasto-plastic fracture mechanics approach based on the J-integral. Figure 7a compares flexural load–displacement curves on pure PLA at different crack propagation levels, along with corresponding images of the crack propagation front, while *J*–*R* curves of pure matrix and of PLA-Ar805-8 sample are reported in Fig. 7b. It is evident that for any given crack propagation value nanofilled sample presents higher *J* values with respect to the neat PLA. Fitting of *J*–*R* curves

Table 5 Tensile impact properties of neat PLA and PLA-Ar805-x nanocomposites ($x = 1 - 24$ vol%)

Sample	σ_{max} (MPa)	ε_b (%)	TEB (MJ m^{-3})
PLA	2.0 ± 0.5	54 ± 9	0.45 ± 0.15
PLA-Ar805-1	2.4 ± 1.0	58 ± 8	0.68 ± 0.16
PLA-Ar805-2	2.9 ± 0.3	77 ± 13	0.77 ± 0.11
PLA-Ar805-4	4.1 ± 0.5	92 ± 22	1.82 ± 0.76
PLA-Ar805-6	4.9 ± 0.2	127 ± 16	2.64 ± 0.27
PLA-Ar805-8	4.6 ± 0.1	129 ± 12	2.67 ± 0.10
PLA-Ar805-16	4.2 ± 0.4	142 ± 10	2.53 ± 0.28
PLA-Ar805-24	3.3 ± 0.1	110 ± 12	1.52 ± 0.13

through the expression reported in Eq. (3) provides the parameters C_1 and C_2 reported in Table 6. A critical *J* value (J_C), conventionally taken in correspondence of a crack propagation of 0.2 mm, is also reported in Table 6. It is interesting to observe that J_C of PLA-Ar805-8 sample is 20 % higher than that of the unfilled matrix, thus confirming that organomodified fumed silica nanoparticles can substantially improve the fracture toughness of PLA.

Creep Stability

In Fig. 8a the creep compliance curves of PLA and PLA-Ar805-8 samples under a creep stress equal to 50 % stress at yield (25.7 MPa) of the neat PLA are compared. It clearly emerges that fumed silica nanoparticles markedly improve the creep stability of the material. Nanoparticles effectively restrict the motion of polymer chains, influencing the stress transfer at a nanoscale, with positive effects on the final creep stability of the material. The stabilizing effect provided by silica nanoparticles is confirmed by the analysis of isochronous curves, reported in Fig. 8b. It is worthwhile to note that for neat PLA isochronous curves slightly deviate from linearity at relatively long creep times (3,600 s), while for nanofilled samples a good linearity is maintained at all creep times up to a stress of 20 MPa. The introduction of silica nanoparticles within the matrix may extend the apparent linearity limit of the viscoelastic behavior of the material. In fact, the chain blocking mechanism provided by silica nanoparticles results to be more effective as the stress level increases and the mobility of polymeric chains is accelerated by the presence of strain-induced free volume. Strong improvements of the creep stability due to fumed silica addition were already observed by our group for other polymeric matrices, such as linear-low density polyethylene [61], poly(methylpentene) [62] and cycloolefin copolymer [63] nanocomposite systems. The Burgers model, widely used to fit creep compliance curves of polymer nanocomposites [71], manifests good fitting capabilities also in the present

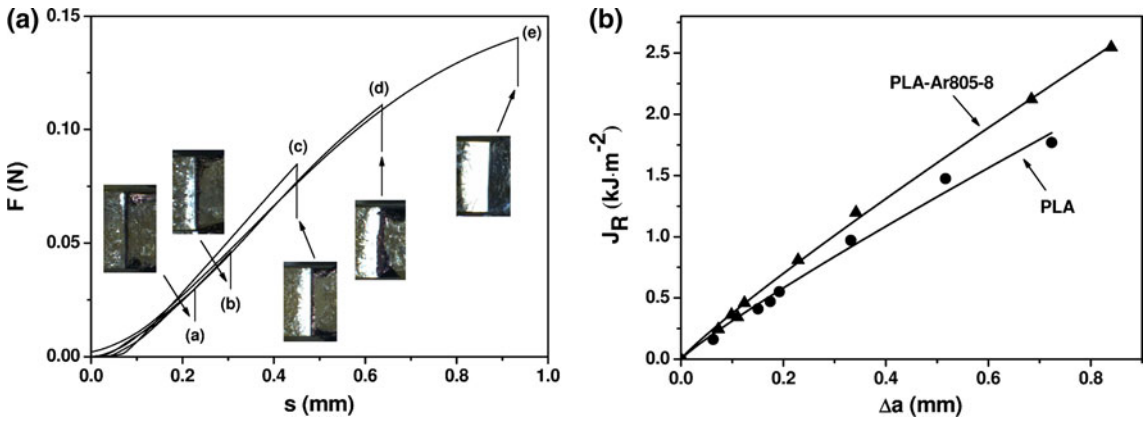

Fig. 7 **a** Representative force-displacement curves of SENB specimens of neat PLA at various crack propagation stages: 0.063, 0.331, 0.516, 1.096, 1.854 mm, **b** *J–R* curves of neat PLA and PLA-Ar805-8 nanocomposite

Table 6 Fitting parameters of *J–R* curves and critical J_c values for neat PLA and PLA-Ar805-8 nanocomposites

Sample	C_1	C_2	J_C (J m^{-2})
PLA	2.45 ± 0.11	0.88 ± 0.05	590
PLA-Ar805-8	3.00 ± 0.05	0.90 ± 0.02	710

case (see continuous lines of Fig. 8a). Considering that the dependency of the creep compliance data from the applied stress is relatively weak, only the curves at an applied stress of 25.7 MPa are reported. From the analysis of the fitting parameters reported in Table 7 it can be concluded that the positive contribution of fumed silica nanoparticles on the creep stability of the material is mostly related to an increase the viscous (η_M, η_K) components of the material behaviour.

Microstructural and Optical Behaviour

In order to correlate the tensile behaviour of the tested materials with their microstructural features, SEM images of the fracture surface of Aerosil® r805 filled nanocomposites are presented in Fig. 9. PLA-Ar805-2 sample (Fig. 9a) is characterized by the presence of isodimensional fumed silica aggregates having a mean dimension of less than 100 nm. This confirms that a good dispersion of the filler is obtained during the melt compounding process. Similar considerations can be extended to 4 and 8 vol% filled nanocomposites (Fig. 9b, c, respectively). In a previous work on cycloolefin copolymer/fumed silica nanocomposites [63], we reported that the introduction of an untreated nanofiller did not produce improvements in the fracture toughness under quasi-static conditions, and TEM images revealed the presence of aggregates having a mean

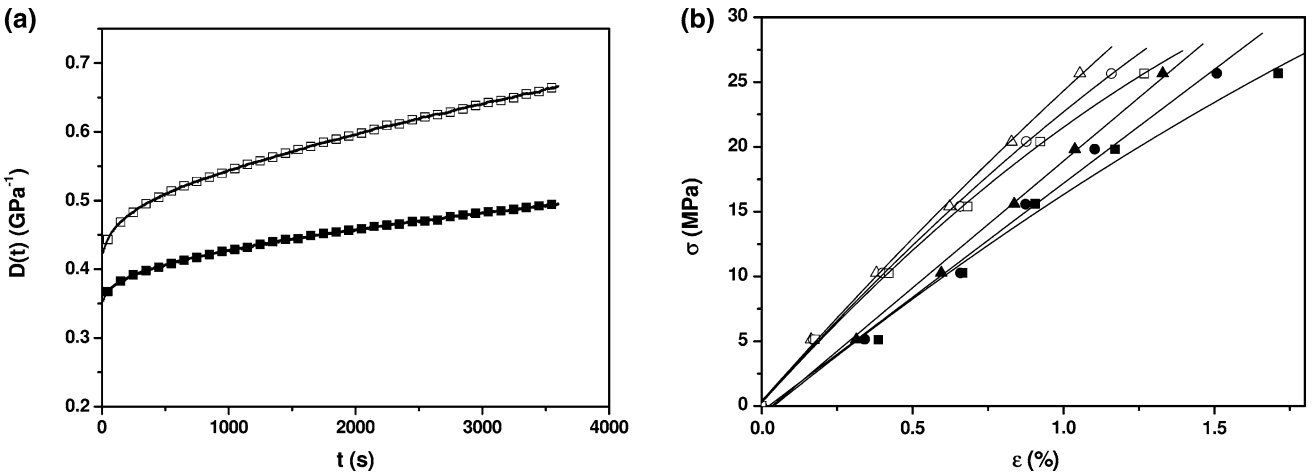

Fig. 8 **a** Creep compliance curves of neat PLA (*square*) and PLA-Ar805-8 nanocomposite (*filled square*) at a creep stress of 25.7 MPa (50 % σ_y of neat PLA), with the fitting lines according to the Burgers model, **b** isochronous curves of (*filled triangle*, *filled circle*, *filled square*) PLA and (*triangle*, *circle*, *square*) PLA-Ar805-8 nanocomposite at 3 different reference times : (*filled triangle*, *triangle*) 600 s, (*filled circle*, *circle*) 1800 s and (*filled square*, *square*) 3,600 s

Table 7 Fitting parameters of the Burger's model for the creep compliances curves of neat PLA and PLA-Ar805-8 nanocomposite at an applied stress of 25.7 MPa (50 % σ_y of neat PLA)

Sample	E_M (GPa)	η_M (Pa s)	E_K (GPa)	η_K (Pa s)
PLA	2.29 ± 0.01	22,200 ± 300	14.7 ± 0.1	5,640 ± 40
PLA-Ar805-8	2.75 ± 0.01	42,000 ± 100	22.1 ± 0.8	10,300 ± 90

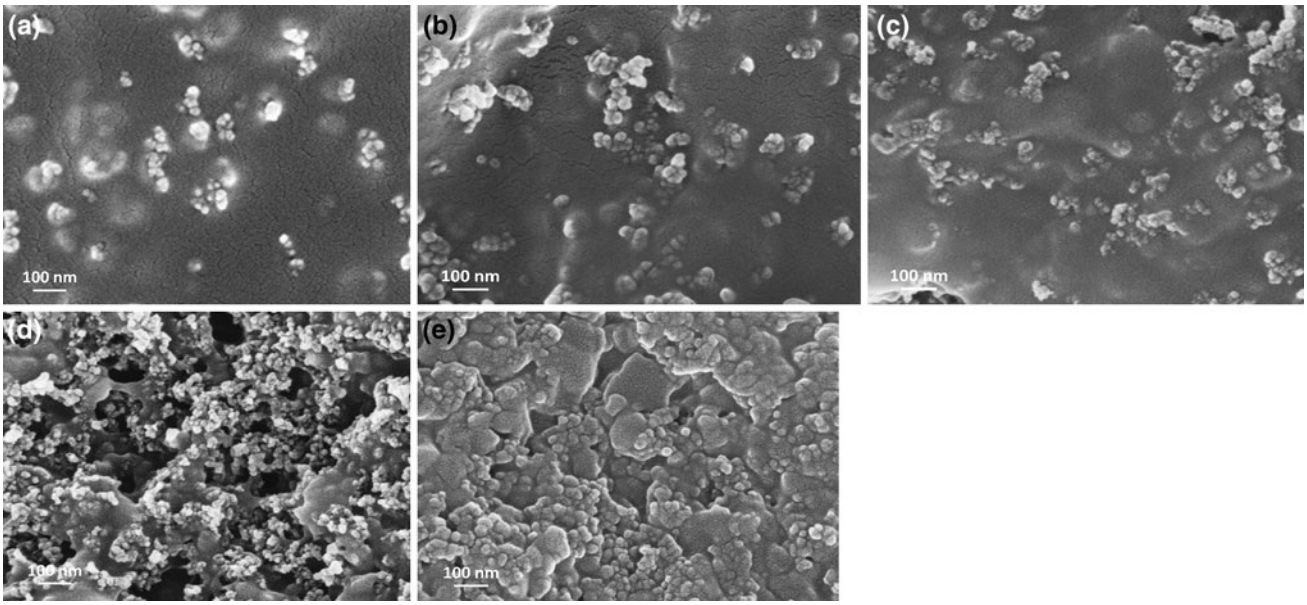

Fig. 9 ESEM images of the fracture surfaces of **a** PLA-Ar805-2, **b** PLA-Ar805-4, **c** PLA-Ar805-8, **d** PLA-Ar805-16, and **e** PLA-Ar805-24 nanocomposites

size higher than 160 nm. In the present case, the presence of the organosilane on the surface of the nanoparticles leads the formation of silica aggregates with lower dimensions, positively affecting the fracture behavior of the material. Similar conclusions were reported by Wichmann et al. [72] in a paper in which the influence of the surface treatment on mechanical behaviour of fumed silica/epoxy resin nanocomposites was investigated. Also in that case the improvement of the dispersability of functionalized silica nanoparticles was attributed to a lowering of the inter-particle attractive forces in the presence of a surface compatibilizer.

As the filler concentration increases (Fig. 9d, e) a higher surface corrugation and the presence of voids can be observed. Such defects may act as crack nucleation sites, thus explaining the detrimental effects on the tensile behaviour of the composites observed at high filler loadings.

Finally, the good dispersion of silica aggregates in the matrix can be related to the optical behaviour of the resulting composites. From the photographs collected in Fig. 10 it is possible to qualitatively assess that the original transparency of the samples is not negatively affected by the presence of fumed silica nanoparticles, neither when an high filler loading is added. Also UV spectroscopy curves reported in Fig. 11 confirm that the loss of transparency due to nanosilica addition is rather limited, even at elevated filler amounts. The retention of the optical transparency displayed by the nanofilled samples at all the investigated compositions can be an important feature if the production of transparent plastic components for the packaging industry is considered as a possible application.

Conclusions

Melt compounded poly(lactic acid)/fumed silica nanocomposites were characterized in order to evaluate the effect of the filler surface area and treatment on the thermal, mechanical and optical behaviour of the resulting materials. While the glass transition temperature and the cristallinity of the PLA matrix were not affected by nanofiller introduction, the tensile mechanical properties were greatly improved. In particular, untreated nanoparticles at high surface area resulted to be more effective in increasing elastic modulus, because of the higher

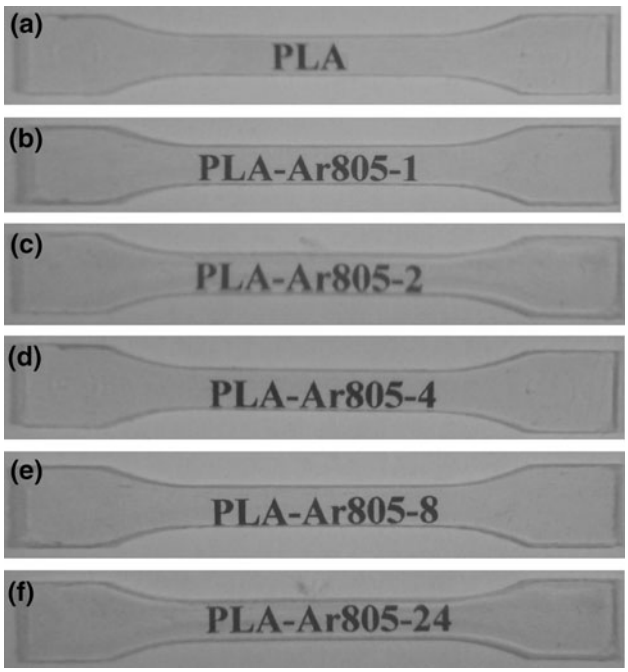

Fig. 10 Photographs for the evaluation of the optical transparency of **a** neat PLA, **b** PLA-Ar805-1, **c** PLA-Ar805-2, **d** PLA-Ar805-4, **e** PLA-Ar805-8, **f** PLA-Ar805-24

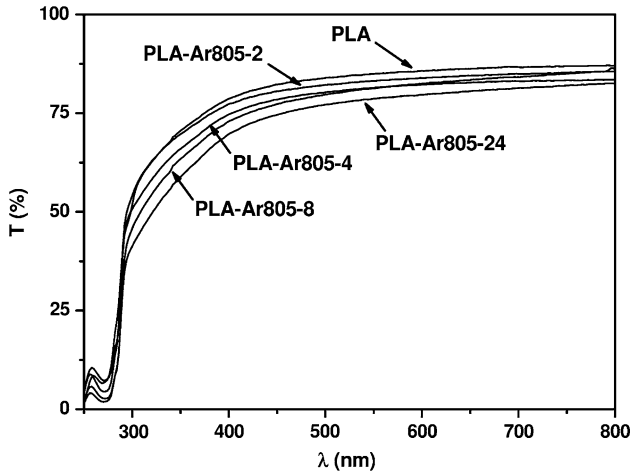

Fig. 11 UV Spectroscopy curves of neat PLA and PLA-Ar805-x ($x = 1 - 24$ vol%) nanocomposites

filler–matrix interaction, while surface treated nanosilica induced tremendous improvements of the ultimate tensile properties. Moreover, fracture mechanics investigations based on the J-integral concept evidenced that fracture toughness of PLA matrix was noticeably improved by addition of functionalized nanosilica. Concurrently, the presence of functionalized fumed silica nanoparticles led to a remarkable improvement of the creep stability, especially under elevated static loads. Finally, the good dispersion of silica aggregates at the nanoscale allowed to maintain the original optical transparency of the matrix even at elevated filler content.

Acknowledgments The authors are indebted to Evonik (Hanau, Germany) for the kind provision of Aerosil nanofillers. Moreover, Lorenzo Moschini (University of Trento) is greatly acknowledged for his help with FESEM analysis.

References

1. Amass W, Amass A, Tighe B (1998) Polym Int 47:89
2. Chiellini E, Solaro R (2003) Recent advances in biodegradable polymers and plastics. Wiley-VCH Verlag, Weinheim
3. Bastioli C (2005) Handbook of biodegradable polymers. Rapra Technology Limited, Shawbury
4. Doi Y, Steinbuchel A (2002) Biopolymers. Polyesters III. Applications and commercial products. Wiley-VCH Verlag, Weinheim
5. Fambri L, Migliaresi C, Kesenci K, Piskin E (2002) Biodegradable polymers. In: Barbucci R (ed) Integrated biomaterials science. Kluwer Plenum Publication, New York, pp 119–187
6. Kulkarni RK, Pani KC, Neuman C, Leonard F (1966) Arch Surg 93:839
7. Auras R, Lim LT, Selke SEM, Tsuji H (2010) Poly(lactic acid): synthesis, structures, properties, processing, and applications. Wiley, Hoboken
8. Lunt J (1998) Polym Degrad Stab 59:145
9. Tsuji H (2002) Polylactide. In: Doi Y, Steinbuchel A (eds) Biopolymers. Polyesters III. Applications and commercial products. Wiley VCH Verlag, Weinheim, pp 129–177
10. Garlotta D (2002) J Polym Environ 9:63
11. Fambri L, Migliaresi C (2010) Crystallization and thermal properties. In: Auras R, Lim LT, Selke SEM, Tsuji H (eds) Poly(lactic acid): Synthesis, structures, properties, processing, and applications. Wiley, Hoboken, NJ, pp 113–124
12. Jamshidi K, Hyon SH, Ikada Y (1988) Polymer 29:2229
13. Fambri L, Bragagna S, Migliaresi C (2006) Macromol Symp 234:20
14. Engelberg I, Kohn J (1991) Biomaterials 12:292
15. Perego G, Cella GD, Bastioli C (1996) J Appl Polym Sci 59:37
16. Renouf-Glauser AC, Rose J, Farrar DF, Cameron RE (2005) Biomaterials 26:5771
17. Auras R, Lim LT (2008) Prog Polym Sci 33:820
18. Jacobsen S, Fritz HG (1999) Polym Eng Sci 39:1303
19. Martin O, Averous L (2001) Polymer 42:6209
20. Ljungberg N, Wesselen B (2002) J Appl Polym Sci 86:1227
21. Labrecque LV, Kumar RA, Dave V, Gross RA, McCarthy SP (1997) J Appl Polym Sci 66:1507
22. Kulinski Z, Piorkowska E, Galeski A, Masirek R (2006) Polymer 47:7178
23. Wypych G (2004) Handbook of plasticizers. ChemTec Publishing, Toronto
24. Wang L, Ma W, Gross RA, McCarthy SP (1998) Polym Degrad Stab 59:161
25. Cabedo L, Feijoo JL, Villanueva MP, Lagaron JM, Gimenez E (2006) Macromol Symp 233:191
26. Barrows TH (1986) Clin Mater 1:233
27. Yuan Y, Ruckenstein E (1998) Polym Bull 40:485
28. Li Y, Shimizu H (2007) Macromol Biosci 7:921
29. Afrifah KA, Matuana LM (2010) Macromol Mater Eng 295:802
30. Higashi S, Yamamuro T, Nakamura T, Ikada Y, Hyon SH, Jamshidi K (1986) Biomaterials 7:183
31. Shikinami Y, Okuno M (1999) Biomaterials 20:859
32. Kesenci K, Fambri L, Migliaresi C, Piskin E (2000) J Biomater Sci Polym 11:617

33. Nazhat SN, Kellomaki M, Tormala P, Tanner KE, Bonfield W (2001) J Biomed Mater Res 58:335
34. Fambri L, Kesenci K, Migliaresi C (2003) Polym Compos 24:100
35. Russias J, Saiz E, Nalla RK, Gryn K, Richtie RO, Tomsia AP (2006) Mater Sci Eng, C 26:1289
36. Kasuga Y, Maeda H, Kato K, Nogami M, Hata K, Ueda M (2003) Biomaterials 24:3247
37. Urayama H, Ma C, Kimura Y (2003) Macromol Mater Eng 288:562
38. Murariu M, Ferreira AD, Degee P, Alexandre M, Dubois P (2007) Polymer 48:2613
39. Pluta M, Murariu M, Ferreira AD, Alexandre M, Galeski A, Dubois P (2007) J Polym Sci, Part B: Polym Phys 45:2770
40. Molnar K, Moczo J, Murariu M, Dubois P, Pukanszky B (2009) Expr Pol Lett 3:49
41. Jain S, Reddy MM, Mohanty AK, Misra AM, Ghosh AK (2010) Macromol Mater Eng 295:750
42. Chang JH, An YU, Cho D, Giannelis EP (2003) Polymer 44:3715
43. Chang JH, An YU, Sur GS (1997) J Polym Sci, Part B: Polym Phys 35:389
44. Lee SY, Chen H, Hann MA (2008) Ind Crop Prod 28:95
45. Lewitus D, McCarthy S, Ophir A, Kenig S (2006) J Polym Environ 14:171
46. McLauchlin AR, Thomas NL (2009) Polym Degrad Stab 94:868
47. Ogata N, Jimenez G, Kawai H, Ogihara T (1997) J Polym Sci, Part B: Polym Phys 35:389
48. Pluta M, Jeszka JK, Boiteux G (2007) Eur Polym J 43:2819
49. Ray SS, Yamada K, Ogami A, Okamoto M, Ueda K (2002) Macromol Rapid Commun 23:943
50. Luo YB, Li WD, Wang XL, Xu DY, Wang YZ (2009) Acta Mater 57:3182
51. Jiang L, Zhang J, Wolcott MP (2007) Polymer 48:7632
52. Cao D, Wu L (2009) J Appl Polym Sci 111:1045
53. Zhang J, Lou J, Ilias S, Krishnamachari P, Yan J (2008) Polymer 49:2381
54. Yan SF, Yin JB, Yang Y, Dai ZZ, Ma J, Chen XS (2007) Polymer 48:1688
55. Zhu A, Diao H, Rong Q, Cai A (2010) J Appl Polym Sci 116:2866
56. Fukushima K, Tabuani D, Abbate C, Arena M, Rizzarelli P (2011) Eur Polym J 47:139
57. Fischer EW, Sterzel HJ, Wegner G (1973) Kolloid-Zeitschrift & Zeitschrift für Polymere 251:980
58. Anderson TL (1995) Fracture Mechanics: Fundamentals and Applications. CRC Press, USA
59. ASTM D6068-10. Standard Test Method for Determining J-R Curves of Plastic Materials
60. Hale GE, Ramsteiner F (2001) J-fracture toughness of polymers at slow speed. In: Moore DR, Pavan A, Williams JG (eds) Fracture mechanics testing methods for polymers, adhesives and composites, vol ESIS Publication 28. Elsevier, Amsterdam, pp 123–157
61. Dorigato A, Pegoretti A, Kolarik J (2010) Polym Compos 31:1947
62. Dorigato A, Pegoretti A (2010) Polym Int 59:719
63. Dorigato A, Pegoretti A, Fambri L, Slouf M, Kolarik J (2011) J Appl Polym Sci 119:3393
64. Hotta S, Paul DR (2004) Polymer 45:7639
65. Morawiec J, Pawlak A, Slouf M, Galeski A, Piorkowska E, Krasnikowa N (2005) Eur Polym J 41:1115
66. Tanniru M, Yuan Q, Misra RDK (2006) Polymer 47:2133
67. Zhang L, Luo M, Sun S, Ma J, Li C (2010) J Macromol Sci, Phys 49:970
68. Naveau E, Dominkovics Z, Detrembleur C, Jerome C, Hari J, Renner K, Alexandre M, Pukanszky B (2011) Eur Polym J 47:5
69. Turcsanyi B, Pukanszky B, Tudos F (1988) J Mater Sci Lett 7:160
70. Szazdi L, Abranyi A, Pukanszky B Jr, Vancso GJ, Pukanszky B (2006) Macromol Mater Eng 291:858
71. Pegoretti A (2009) Creep and fatigue behaviour of polymer nanocomposites. In: Karger-Kocsis J, Fakirov S (eds) Nano- and micromechanics of polymer blends and composites. Carl Hanser Verlag GmbH & Co. KG., Munich, pp 301–339
72. Wichmann MHG, Cascione M, Fiedler B, Quaresimin M, Schulte K (2006) Compos Interface 13:699